NJC

ROYAL SOCIETY OF CHEMISTRY

PAPER

View Article Online
View Journal | View Issue

Cite this: *New J. Chem.*, 2025, 49, 11778

Development of polymeric ionic poly(VBC-*co*-VI) nanoparticle incorporated thin film nanocomposite membranes for dye and salt rejection†

Nidhi Regina Mendonca, [a] Arun M. Isloor *[a] and Ramin Farnood[b]

Received 29th January 2025,
Accepted 16th April 2025

DOI: 10.1039/d5nj00404g

rsc.li/njc

Water is an important life-sustaining liquid. However, due to the current anthropogenic activities, this resource is diminishing. This work explores a method for the potential reuse of textile wastewater containing salts by utilization of thin film composite (TFC) membranes fabricated by means of interfacial polymerization on a macroporous membrane substrate composed of 15% polysulfone (PSf). A relatively lesser known variety of nanoparticles termed ionic polymeric nanoparticles were integrated into the dense polyamide (PA) layer. The ionic poly(VBC-*co*-VI) nanoparticles were synthesized in the laboratory *via* quaternary precipitation polymerization (QPP) of the monomers 1-vinyl imidazole (VI) and 4-vinybenzyl chloride (VBC) by the utilization of 2,2′-azobis(2-methylpropionitrile) (AIBN) as the free radical initiator in the solvent acetonitrile (ACN) in a single step. The synthesized nanoparticles existing in the PA layer improved the water permeability as well as the rejection capacity of the membranes. The fabricated membranes showed a dye rejection of 98% for Reactive Black 5 and >95% for Sunset Yellow FCF having a concentration of 100 ppm. The salt rejection for NaCl, MgCl, Na_2SO_4 and $MgSO_4$ at 1000 ppm concentration was found to be 36%, >50%, 85% and 85%, respectively.

1. Introduction

Life on Earth is possible mainly due to two compounds, molecular oxygen and water. Water is essential for living organisms since biochemical reactions in the body utilize water as a solvent. However, in recent years, the quality of water fit for human consumption has dwindled due to the presence of pollutants. A plethora of methods are available for the treatment of wastewater which include processes like adsorption,[1] sedimentation,[2] coagulation,[3] flocculation,[4] ion exchange[5] and membrane technology.[6] In comparison to the other techniques available for water treatment, membrane technology emerges as the most suitable method, because of its versatility, propensity towards efficient and continuous separation of large volume of feed, lack of secondary product formation and effective low cost.[7]

Nanofiltration (NF) and reverse osmosis (RO) membranes are employed for the exclusion of heavy metals and ions from wastewater.[8] NF membranes have certain advantages over RO membranes in that the divalent ions are removed preferentially in the presence of monovalent ions and NF membranes operate at a relatively lower pressure compared to RO membranes, thereby reducing the operating cost significantly.[9] NF membranes can help in the separation of salts, associated organic compounds and dyes from wastewater in a single step.[10,11] These membranes can help in the rejection of not only larger dye molecules but also salts in textile wastewater. Hence, it is possible to recycle water from the textile wastewater. This is especially true for reactive dyes and azo dyes which are water soluble and cannot be easily removed by coagulation or flocculation.[12] The use of NF membranes ensures the removal of both the dyes as well as the salts.

Polysulfone (PSf) structurally consists of aryl groups linked *via* ether (–O–) and sulfone ($–SO_2–$) groups.[13] PSf is stable at high temperatures and possesses appreciable mechanical strength.[14] However, PSf has a downside of hydrophobicity which can be overcome by various methods like the formation of blend membranes,[15] incorporation of additives to give mixed matrix membranes,[16] chemical grafting[17] and by fabrication of thin film composite (TFC) membranes.[18] These methods help to improve the permeability of PSf as a consequence of increased hydrophilicity.

[a] *Membranes and Separation Technology Lab, Department of Chemistry, National Institute of Technology Karnataka, Surathkal-575025, India. E-mail: isloor@yahoo.com*
[b] *Department of Chemical Engineering and Applied Chemistry, University of Toronto, Canada*

† Electronic supplementary information (ESI) available. See DOI: https://doi.org/10.1039/d5nj00404g

NF membranes can be prepared *via* interfacial polymerization (IP) between the aqueous layer containing piperazine (PIP) and the organic layer composed of cyclohexane containing a known concentration of trimesoyl chloride (TMC) and nanoparticles, on a membrane support which is macroporous in nature.[19] The resulting polyamide (PA) layer is dense and selective and the membrane is termed as the thin film nanocomposite (TFN) membrane. The support membrane primarily improves the mechanical strength of the PA layer whose thickness is less than 200 nm.[20] The PA layer is the selectively permeable barrier which is responsible for the permeability of water and the rejection of solutes. The properties of the PA layer can be tuned using a plethora of techniques like the utilization of additives in the solutions used for IP[21] by using different combinations of solvent, co-solvent or the support membrane[22] and by varying the post treatment method.[23] This work focuses on the use of additives in the PA layer in order to enhance the property of the TFC, giving rise to TFN membranes.

The additives used in the fabrication of TFN membranes include nanosheets,[24,25] metal organic frameworks (MOFs),[26,27] MXenes[28] and nanoparticles.[29,30] In this work, a class of nanoparticles termed ionic polymeric nanoparticles was employed. The incorporation of ionic moieties in the membrane arising from the addition of ionic nanoparticles induces a net charge on the membrane.[31] As a result of the net charge possessed by the membrane, a phenomenon termed as Donnan exclusion occurs, in which the ions having charges similar to the substrate are repelled while the ions of the opposite charge pass through.[32,33] This phenomenon takes place in tandem with the molecular sieving associated with pressure-driven membrane processes like nanofiltration.

Syed *et al.* first reported the synthesis of polymeric ionic nanoparticles *via* quaternization precipitation polymerization (QPP) utilizing the Menshutkin reaction.[34] The reaction was carried out under reflux conditions without using any cross linker. The ionic nanoparticles were incorporated in the fabrication of mixed matrix membranes for the purpose of oil/water separation. From the available literature, it can be observed that the utilization of ionic polymeric nanoparticles for the fabrication of TFN membranes and their subsequent analysis in the rejection study of dyes and salts has not been carried out before. Since the ionic nanoparticles possess a charge, which is imparted to the fabricated membrane, it was assumed that the increased surface charge of the membranes helps in the rejection of ions. Moreover, the synthesis of a diversity of ionic nanoparticles has not been well reported in the literature.

The dye and salt rejection using TFC membranes has been reported before using other additives. Prabhakar *et al.* fabricated TFC membranes containing MIL-53(Fe)-zwitterionic brushes over a PVDF support which displayed Reactive Black 5 and Sunset Yellow FCF rejection of 96.23% and 94.04%, respectively.[21] Mahadevaprasad *et al.* fabricated TFC membranes possessing Mn-aminoclay additives over a PES support, which showed 60.99% rejection of $MgSO_4$ and 45.99% rejection of NaCl.[35] Zhang *et al.* fabricated polyester-based nanofiltration membranes incorporated with a molecule mimicking capsaicin which showed rejection of NaCl and Na_2SO_4 of 4% and 83.8%.[36] Dong *et al.* fabricated nanofiltration membranes containing a polyester membrane support incorporated with single walled carbon nanotubes (SWCNTs) which showed rejection of 24.3%, 2.9%, 91.8% and 23.2% respectively for NaCl, $MgCl_2$, Na_2SO_4 and $MgSO_4$.[37]

In this work, previously unreported poly(VBC-*co*-VI) ionic nanoparticles were synthesized using 1-vinyl imidazole (VI) and 4-vinybenzyl chloride (VBC) as monomers using the QPP method. The reaction was carried out in 20 mL of acetonitrile (ACN) using 2,2′-azobis(2-methylpropionitrile) (AIBN) as the free radical initiator. The nanoparticles were then incorporated into the PA layer fabricated over the PSf membrane *via* interfacial polymerisation. Since these nanoparticles possess a charge, it was assumed that the incorporation of the nanoparticles in the PA layer would help in the rejection of charged species like ions and dyes *via* electrostatic interactions. The fabricated membranes were tested for their rejection towards dyes Reactive Black 5 and Sunset Yellow FCF having 100 ppm concentration and salts NaCl, MgCl, Na_2SO_4 and $MgSO_4$ having 1000 ppm concentration.

2. Materials and methods

2.1 Materials

Polysulfone (PSf, P-3500 Udel) was purchased from Solvay chemicals, 4-vinybenzyl chloride (VBC, 90%), 1-vinyl imidazole (VI, $\geq$99%), piperazine (PIP, 99%), Reactive Black 5 (RB5, $\geq$50%) and Sunset Yellow FCF (SY FCF, 90%) were procured from Sigma-Aldrich. Acetonitrile (ACN, 99.9%), cyclohexane ($>$99%), polyethylene glycol (PEG) 200 and 400 Da were procured from Merck, trimesoyl chloride (TMC, $>$98%) was procured from Tokyo Chemical Industry, bovine serum albumin (BSA, $\geq$98%), sodium sulphate (Na_2SO_4, 99%), and PEG 1000 Da were procured from Himedia, sodium chloride (NaCl, 99.5%) was purchased from Spectrum Chemical Mfg. Corp., 2,2′-azobis(2-methylpropionitrile) (AIBN, 98%) and magnesium chloride ($MgCl_2$, 99%) were procured from Spectrochem Pvt. Ltd, magnesium sulphate ($MgSO_4$, 99%) was procured from NICE Chemicals Pvt. Ltd, *N*-methyl pyrrolidone (NMP, 98%), PEG 600 Da and poly(vinylpyrrolidone) (PVP) from Loba Chemie, and ultrapure (Type 1) deionized water was acquired from Millipore Direct-Q® 3.

2.2 Methods

2.2.1 Synthesis of nanoparticles. The synthesis of the nanoparticles (Fig. 1) was carried out employing the method reported by Syed *et al.*[34] In short, VBC (0.78 g, 5.1 mmol) was taken in a 50 mL single neck RBF to which VI (1.0 g, 10.6 mmol) was added. To the same reaction vessel, AIBN (0.02 g, 0.12 mmol) was added, succeeded by the addition of 20 mL of ACN. The dissolved oxygen in the reaction mixture was displaced by purging the reaction mixture with N_2 gas for 10 minutes. The reaction mixture was heated to 100 °C after

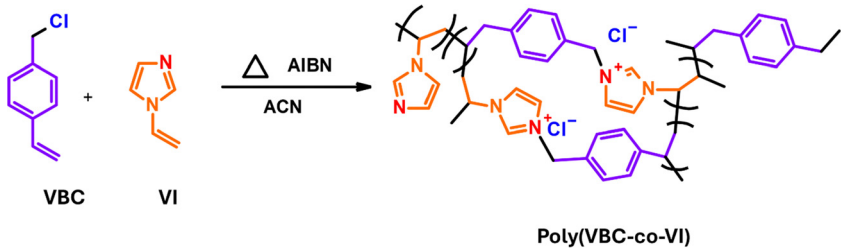

Fig. 1 Scheme for the synthesis of poly(VBC-*co*-VI) nanoparticles.

connecting a Dean–Stark apparatus. The heating was stopped after 5 hours and the reaction mixture underwent stirring for an additional hour to bring it to room temperature. The product was isolated by centrifugation and washed twice with 20 mL of ACN to get rid of any unreacted monomers and was later dried overnight at 60 °C under vacuum (−600 mm Hg). The yield obtained was 0.8565 g.

2.2.2 Fabrication of support membranes. The support layer for the TFN membranes was fabricated in the laboratory. 1 wt% PVP was taken in a dope bottle to which 84 wt% NMP was added. After the PVP dissolved in the solvent, 15 wt% PSf granules were introduced to the solution and the resulting mixture was stirred for 24 hours at 60 °C to form a homogeneous polymer solution referred to as the dope solution. After degassing for 30 minutes and keeping in an oven at 60 °C for 3 hours, the dope solution was spread on a glass plate using an automated K-control coater (purchased from UK). The plate was submerged in a coagulation bath containing deionized water and the membrane was left undisturbed for 24 hours for the phase inversion to complete. After 24 hours, the membrane was ready for use as the support for TFN membranes.

2.2.3 Fabrication of thin film nanocomposite membranes. The dense polyamide (PA) layer of the thin film nanocomposite membrane was fabricated using an interfacial polymerization method. The poly(VBC-*co*-VI) nanoparticles were homogenised in the organic phase consisting of cyclohexane and 0.2 wt% TMC. The compositions were 0.05, 0.1 and 0.15 wt% of cyclohexane. These were labelled as TFN-1, TFN-2 and TFN-3, respectively (Table 1). In order to ensure the even dispersion of the nanoparticles in the solvent, each solution composition was sonicated at 40 kHz for 30 minutes in an ultrasonicator. The neat thin film composite membrane was labelled as TFC. The aqueous layer was composed of 2 wt% PIP.

The fabrication of the TFN membranes was carried out as follows. First, the PSf support layer was positioned on a glass plate and the excess water was squeezed out using a rubber roller. A rubber gasket with a circular cutout was placed over the membrane and secured with stainless steel clips. Then, 10 mL of the aqueous solution was poured into the cutout and allowed to stand for 10 minutes, after which the aqueous layer was discarded. The rubber gasket was removed and the excess solution was removed using a rubber roller. After placing and securing the rubber gasket, 10 mL of the organic solution was poured and allowed to coat for 2 minutes. The surplus organic solution was disposed and the resulting TFN membrane was kept in an oven at 60 °C for 15 minutes. After drying, the TFN membranes were submerged in DI water for a day before further testing.

Table 1 Table displaying the data for the fabrication of the PA layer of TFN

Code	TMC (g)	Poly(VBC-*co*-VI) (wt%)	Poly(VBC-*co*-VI) weight (g)	Cyclohexane (mL)
TFC	0.015	—	—	10
TFN-1	0.015	0.025	0.005	10
TFN-2	0.015	0.05	0.01	10
TFN-3	0.015	0.1	0.02	10

2.2.4 Characterization

2.2.4.1 Poly(VBC-co-VI). The nanoparticle morphology was ascertained from the images obtained with the help of the scanning electron microscope (SEM), and the elements present in the nanoparticles were determined using EDS (Apreo 2, Thermo Fisher Scientific). The 2D image of the nanoparticles was obtained using a transmission electron microscope (TEM), and the crystalline structure of the nanoparticles was determined using selected area electron diffraction (SAED) (Tecnai G2 F20 S-TWIN, FEI). The nanoparticle crystallinity was further confirmed from X-ray diffraction (XRD) (MiniFlex 600, Rigaku). The functional group present in the nanoparticle was determined using FTIR in ATR mode (Nicolet Summit X, Thermo Fisher Scientific) from 400 to 4000 cm^{-1} using 32 sample scans. The surface area, pore volume and pore diameter were determined using BET analysis (Mini X, BELSORP). The charge possessed by the nanoparticles was determined using the zeta potential, and the hydrodynamic diameter was ascertained from dynamic light scattering (DLS) (Zetasizer Nano Serial number: MAL1211069, Malvern Panalytical). Thermogravimetric analysis (TGA) was carried out using TGA 4000, Perkin-Elmer in order to determine the thermal stability of the nanoparticles.

2.2.4.2 Membrane. The SEM images of the membrane surface were obtained using Carl Zeiss EVO MA18 and the elemental analysis was carried out using Oxford EDS (X-Act). The water contact angle was measured at room temperature using a contact angle analyser (DMe-211Plus, Kyowa) by the utilization of the sessile droplet mode. The surface roughness of the thin film composite membranes was ascertained *via* atomic force microscopy (AFM) (Flex-Axiom AFM, Nanosurf). The membrane zeta potential was ascertained using a SurPASS 1, Anton Paar zeta potential analyser over the pH range of 2 to 10.

2.2.4.2.1 Permeability and rejection studies. The fabricated thin film composite membranes were subjected to pure water permeability (PWP) studies by employing a cross-flow filtration set-up. A circular membrane area of 28.27 cm^2 was employed for the study. The membranes were first compacted at 5 bar pressure for 30 minutes, in order to open up the pores and remove any excess NMP in the pore cavities. Later, the PWP was determined at 4 bar pressure. Eqn (1) was employed for the calculation of permeability (J, L m^{-2} h^{-1} bar^{-1}).

$$J = \frac{V}{A \times t \times P} \quad (1)$$

where 'V' corresponds to the water volume (L) passing through the membrane over a time period 't' (h) 'A' corresponds to the membrane area (m^2) 'P' corresponds to the operating pressure (bar).

The filtration setup which was employed for permeability studies was utilized for the rejection studies of the dyes and salts. The permeate was collected at 4 bar pressure after the completion of membrane compaction at 5 bar pressure for 30 minutes. RB5 and SY FCF dyes were used for the dye rejection study wherein the dye concentration was 100 ppm. The permeate along with the respective feed was analyzed using UV spectroscopy (Analytical Technologies Limited, Spectro UV 2080+). The salts used in the rejection study were NaCl, MgCl, $NaSO_4$ and $MgSO_4$ at 1000 ppm concentration. The permeate and the feed solutions obtained after the study were analyzed using a TDS instrument (TDSTestr11+, Eutech Instruments). The percentage of rejection of the solutes by the series of membranes was calculated using eqn (2).

$$\text{Rejection percentage} = \left(1 - \frac{C_p}{C_f}\right) \times 100 \quad (2)$$

where 'C_p' corresponds to the permeate concentration and 'C_f' corresponds to the feed concentration.

2.2.4.2.2 Study of porosity and water uptake of the membranes. The thin film composite membranes were cut into squares of 2 × 2 cm^2 and allowed to rest in deionized water for 24 hours. The wet weight of the membranes was then measured after removing the excess water on the membranes using tissue paper. The membrane pieces were then kept for drying in a hot air oven at a temperature of 60 °C for 24 hours. Then the dry weight was determined and the water uptake of the membranes was calculated using eqn (3).

$$\text{Percentage water uptake} = \frac{W_w - W_d}{W_d} \times 100 \quad (3)$$

where 'W_w' corresponds to the wet weight of the membrane and 'W_d' corresponds to the dry weight of the membrane.

The membrane porosity (ε) was calculated using eqn (4).

$$\varepsilon = \frac{W_w - W_d}{A \times l \times d_w} \times 100 \quad (4)$$

where 'A' corresponds to the membrane area taken (cm^2), 'l' corresponds to the thickness of the membrane (cm), and 'd_w' is the density of pure water (g cm^{-3}).

2.2.4.2.3 Antifouling study. The improvement in the antifouling property after the addition of nanoparticles to the PA layer was examined *via* the degree of adsorption of BSA, which is a well known foulant. A square piece of the fabricated TFN membrane of 2 × 2 cm^2 was placed in a beaker containing a BSA of 0.8 mg mL^{-1} concentration. The solution was collected after 24 hours and its concentration was analysed using a UV spectrophotometer. The degree to which BSA was adsorbed on the membrane (Q, μg cm^{-2}) was calculated using eqn (5).

$$Q = \frac{(C_1 - C_2) \times V}{A} \times 1000 \quad (5)$$

where 'C_1' corresponds to the feed BSA concentration, 'C_2' corresponds to the BSA concentration after adsorption, 'V' corresponds to the volume of the BSA solution taken (mL), and 'A' corresponds to the total surface area including both sides of the membranes (cm^2).

3. Results

3.1 Poly(VBC-*co*-VSPI)

The SEM image of the nanoparticles shows a cauliflower-like morphology (Fig. 2(a)). The average diameter of the nanoparticles was 125 nm. The nanoparticles appear to be aggregated most probably due to the electrostatic interactions between the nanoparticles. The EDS mapping (Fig. 2(b)) of the nanoparticles proves that the free radical polymerization reaction between VBC and VI has taken place due to the presence of Cl and N peaks. The data show an appreciable amount of O, indicating the presence of the water molecules, which are adsorbed on the surface of the nanoparticles.

The nanoparticles possessed a zeta potential of 23.8 mV at pH 7 (Fig. S2A, ESI†). The positive value of the zeta potential could be attributed to the presence of the quaternary ammonium groups. The hydrodynamic diameter was inferred from DLS which was found out to be 4969 nm (Fig. S2B, ESI†). The increase in the hydrodynamic diameter compared to the particle size could be due to the formation of a hydration layer around the nanoparticles.

The TEM images showed the 2D version of the cauliflower morphology (Fig. 2(c)). From the SAED pattern (Fig. 2(d)) of the poly(VBC-*co*-VI) nanoparticles, it is evident that the nanoparticles are amorphous in nature due to the absence of bright spots and the presence of diffuse concentric rings.[38] The presence of a single diffuse peak at 23.28° in the XRD spectrum confirms the amorphous nature of the nanoparticles (Fig. 2(e)).

From the BET analysis, the pore diameter of the nanoparticles was determined to be 13.292 nm. The pore volume was 1.7559 cm^3 g^{-1} and the BET surface area was 7.6425 m^2 g^{-1}. The type of the hysteresis loop (Fig. S3, ESI†) observed was of the H1 type with ink bottle pores usually seen in mesoporous materials with uniform pores.[39]

The FTIR spectrum helped in the determination of the functional groups present in poly(VBC-*co*-VI) nanoparticles (Fig. 2(f)). The peak at 3378 cm^{-1} corresponds to O–H stretching resulting from water adsorbed on the nanoparticles, while

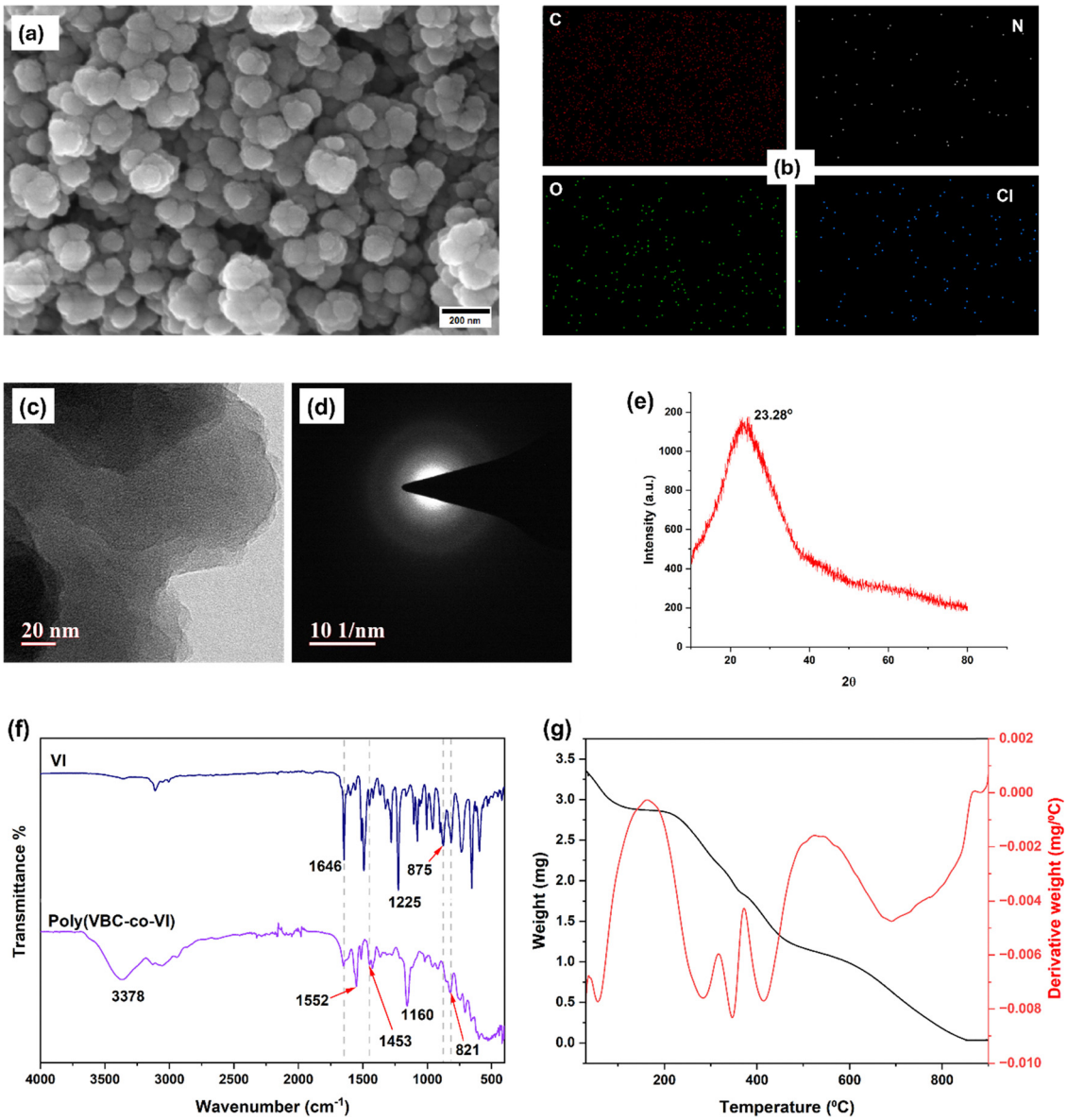

Fig. 2 (a) FESEM image of the poly(VBC-*co*-VI) nanoparticles, (b) EDS images of the poly(VBC-*co*-VI) nanoparticles, showing the presence of C, N, O and Cl, (c) TEM image and (d) SAED pattern of poly(VBC-*co*-VI), (e) XRD peak of poly(VBC-*co*-VI), (f) FTIR spectrum of VI and poly(VBC-*co*-VI), (g) TGA and DTA of poly(VBC-*co*-VI) nanoparticles.

the peak at 1453 cm^{-1} corresponds to the C–H bending vibration of the methylene group. The peaks at 1646 cm^{-1} and 875 cm^{-1} correspond to the C=C vinylidene stretching and bending vibrations, respectively, in VI which is reduced/absent in the nanoparticles implying that the polymerization reaction has been completed.[40] The peak at 1552 cm^{-1} in the nanoparticle corresponds to the aromatic stretch arising from the benzene ring of the cross linker VBC. The peak corresponding to C–N stretching which lies at 1225 cm^{-1} in VI has shifted to 1160 cm^{-1} in the nanoparticle as the vinylidene moiety has been converted to a single bond. The peak at 821 cm^{-1} can be correlated to the C–H bending in the imidazole moiety.[41]

The determination of the thermal stability of the nanoparticles was carried out using TGA (Fig. 2(g)). Three steps were visible in the thermogram. There is a loss of water adsorbed on the nanoparticle taking place from 50 °C to 100 °C which can be observed as the first step. From about 203 °C to 452 °C, another step was seen, which can be correlated to the loss of quaternary ammonium groups. The last step from around 600 °C to 850 °C corresponds to the complete degradation of the nanoparticle. Hence the poly(VBC-*co*-VI) ionic nanoparticles have good thermal stability up to 200 °C.

3.2 Membranes

3.2.1 Membrane surface morphology. The surface SEM of the fabricated membranes revealed the manner of distribution of the nanoparticles on the membrane surface as shown in Fig. 3. The neat TFC membrane has a relatively clear top surface

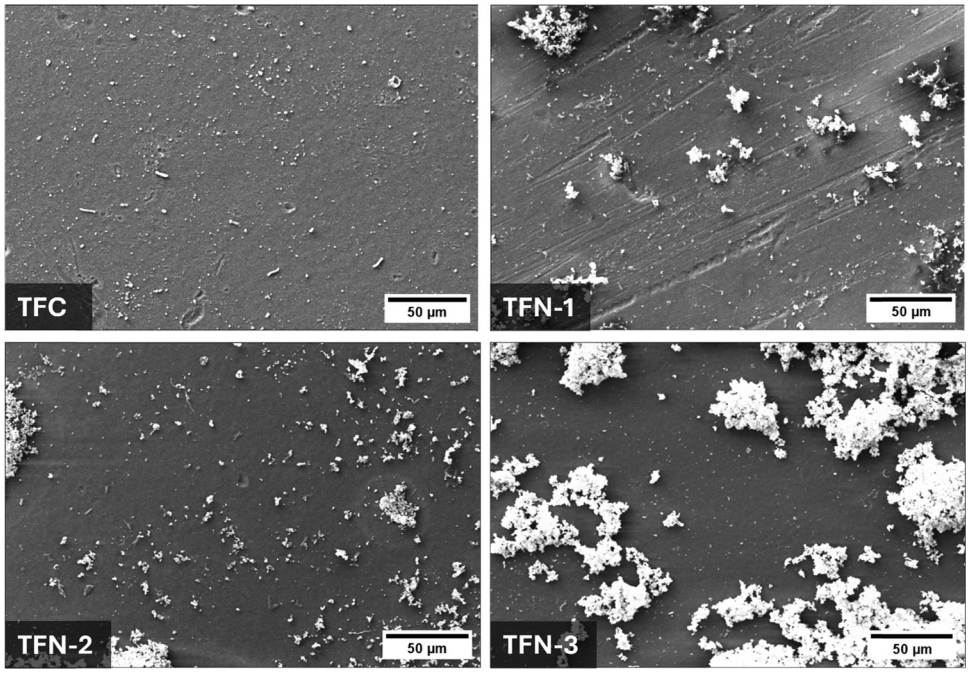

Fig. 3 SEM images of the surface of the fabricated TFN membranes.

as the nanoparticles are not present. As the quantity of the nanoparticles in the organic component increases, there is an aggregation of the nanoparticles on the surface of the membranes. This, in turn, helps to increase the permeability of the membranes because the ionic polymeric nanoparticles can adsorb a layer of water on their surface.

The presence of oxygen in the EDS mapping data (Fig. S5, ESI†) can be attributed to the oxygen from the amide linkage as well as the water adsorbed on the nanoparticles, which was ascertained from the SEM as well as the FTIR analysis of the nanoparticles.

The mechanism for the adsorption of water molecules by the nanoparticles could be attributed to the hydrogen bonding between the lone pair possessing nitrogen of the imidazole moiety with the hydrogen from the water molecule. The starting material VI is quite hygroscopic due to its affinity towards water molecules because of facile hydrogen bond formation. The representation of this mechanism has been given in the ESI† (Fig. S6).

3.2.2 Pure water permeability study. The study of the permeability of pure water through a membrane is crucial in assessing the hydrophilicity of the membrane. Generally, nanofiltration membranes possess lower permeability compared to microfiltration and ultrafiltration membranes and this is evident from the data obtained from the permeability studies of the fabricated membranes. From Fig. 4a and c, it can be observed that the pure water permeability is almost similar in the case of TFN-2 and TFN-3 membranes (4.81 L m^{-2} h^{-1} bar^{-1} and 4.70 L m^{-2} h^{-1} bar^{-1}, respectively) which implies that the poly(VBC-*co*-VI) nanoparticles are effective in increasing the hydrophilicity of the TFN membranes compared to the TFC membrane (1.85 L m^{-2} h^{-1} bar^{-1}). However, from Fig. 4b and d, it can be observed that the permeability of 800 ppm BSA is greater in the case of TFN-3 (5.0 L m^{-2} h^{-1} bar^{-1}) compared to TFN-2 (4.39 L m^{-2} h^{-1} bar^{-1}), which shows that the increase in the addition of the ionic polymeric nanoparticles helps to improve the permeability of the TFN membranes by the formation of channels in the PA layer.[42]

A similar trend is observed in the case of dye permeability of the membranes, wherein the TFN 3 membrane showed better permeability compared to the TFN 2 membranes (Fig. S7, ESI†). However, the performance of a membrane is determined by the permeability and selectivity; hence, the rejection study discusses the selectivity of the fabricated membranes.

3.2.3 Rejection study. The rejection study of the membranes using dyes was carried out using RB5 and SY FCF having a concentration of 100 ppm. Since both the dyes are anionic in nature, it is assumed that the attractive forces between the negatively charged dye molecules and the ionic nanoparticles having a positive zeta potential are responsible for the rejection of the dye molecules by the TFN membranes. From Fig. 5, it can be observed that the TFN-2 membrane shows better rejection of both RB5 (98.12%) and SY FCF (95.86%) compared to the neat TFC membrane (89.68% for RB5 and 79.25% for SY FCF). This shows that the ionic nanoparticles enhance the dye rejection capability of the membranes. However, it can be observed that in the TFN-3 membrane, the dye rejection is lower (86.24% for RB5 and 91.18% for SY FCF), which can be attributed to aggregation of the nanoparticles on the PA layer, which enhances the hydrophilicity but reduces the selectivity of the membrane.

From Fig. 6, it can be observed that the fabricated membranes show better rejection of Na_2SO_4 and $MgSO_4$ compared to NaCl and $MgCl_2$. Furthermore, $MgCl_2$ shows higher rejection

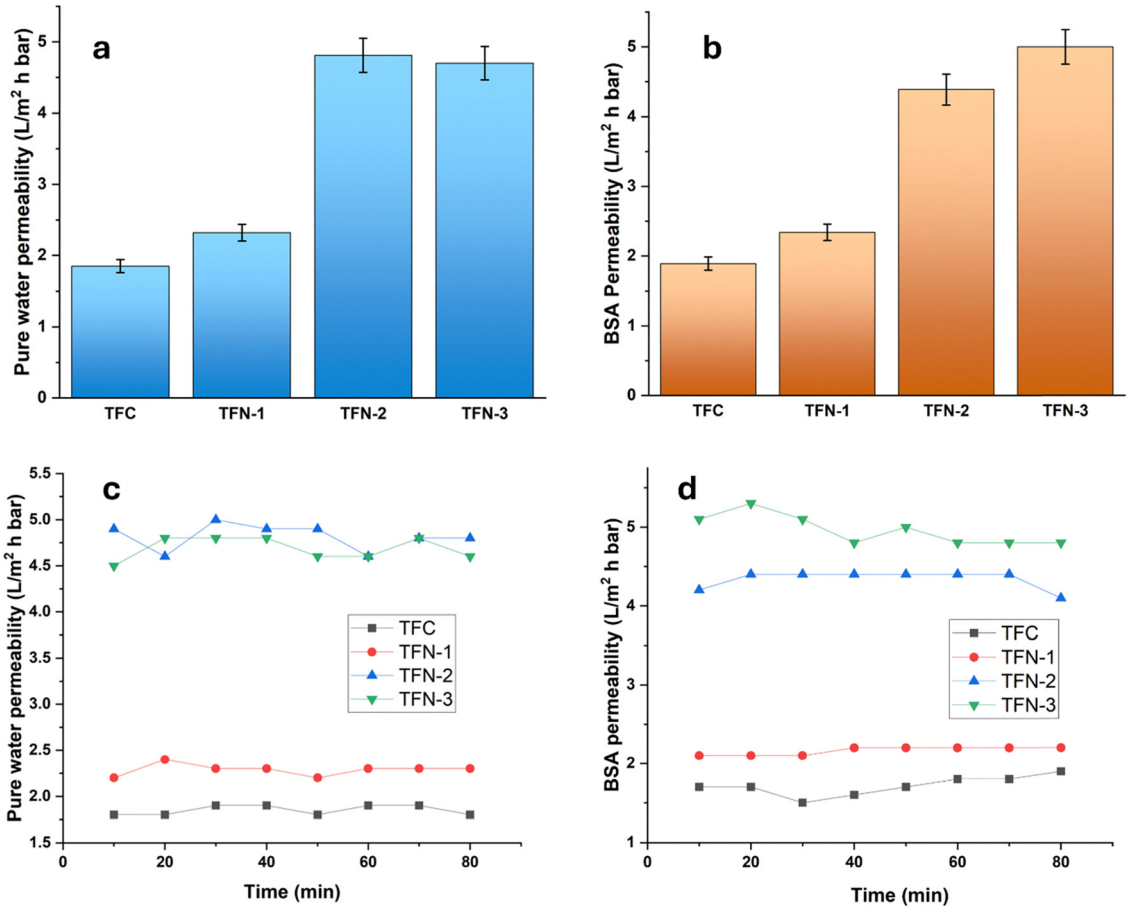

Fig. 4 Overall permeability of (a) water (b) BSA and time dependent permeability of (c) water and (d) BSA of the fabricated membranes.

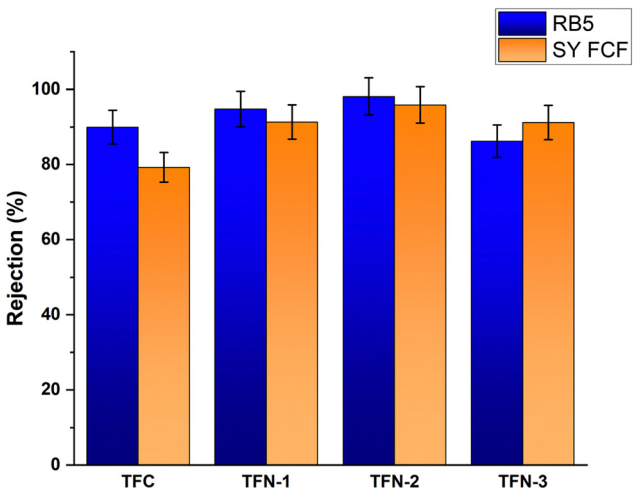

Fig. 5 Graph displaying the dye rejection by the membranes.

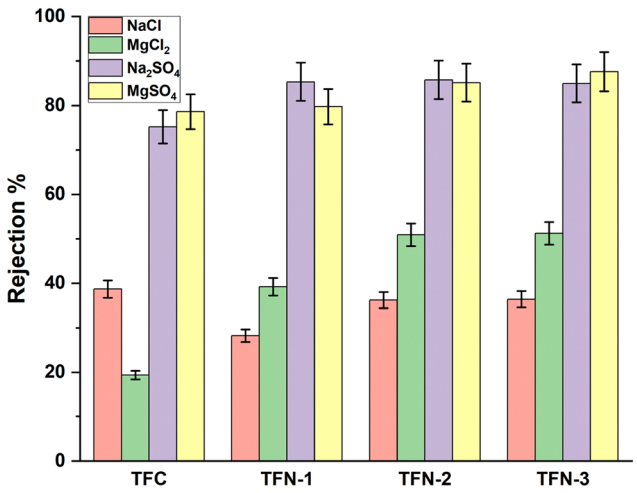

Fig. 6 Graph displaying the salt rejection by the membranes.

compared to NaCl which can be attributed to the higher charge of Mg^{2+} and SO_4^{2-}, resulting in a larger hydration shell, leading to better rejection of the larger species.[43] The TFN 2 membrane shows a better rejection of 50.93% for $MgCl_2$, 85.75% for Na_2SO_4 and 85.15% for $MgSO_4$ compared to the neat TFC membrane which shows a rejection of 19.37% for $MgCl_2$, 75.21% for Na_2SO_4 and 78.63% for $MgSO_4$.

The greater rejection of Na^+ ions in the case of NaCl rejection of the TFC membrane (38.68%) compared to the TFN 2 membrane (36.22%) can be explained by the amount

Table 2 Table displaying the pure water uptake, porosity and contact angle of the fabricated membranes

Membrane	Pure water uptake (%)	Porosity (%)	Contact angle (degree)
TFC	74.53	33.71	42.8
TFN-1	76.87	73.31	41.6
TFN-2	79.94	74.73	29.8
TFN-3	74.32	61.68	29.2

Table 3 The surface roughness parameters of the membrane obtained from AFM analysis

Membrane	R_a (nm)	R_q (nm)	R_{max} (nm)
TFC	9.65	12.01	39.73
TFN-1	6.62	7.60	25.35
TFN-2	14.68	18.71	99.18
TFN-3	17.95	23.96	97.18

of water adsorbed on the dense layer. The diffusion of the ions decreases as the water present on the membrane matrix decreases.[44] Since the nanoparticles show a tendency towards the adsorption of water molecules on their surface, the nanocomposite membranes are more permeable towards NaCl compared to the neat TFC membrane.

3.2.4 Water uptake, porosity and water contact angle. The incorporation of poly(VBC-*co*-VI) nanoparticles into the PA layer of the TFN membranes helped in increasing the porosity of the dense top layer, which in turn increased the pure water flux. From Table 2, it can be observed that the porosity of the TFN-2 membrane (74.73%) is slightly more than double that of the TFC membrane (33.71%). The TFN-1 and TFN-3 membranes showed porosities of 73.31% and 61.68%, respectively, which were significantly greater than that of the neat TFC membrane.

The pure water uptake of the TFN-2 (79.94%) membrane was relatively greater than that of TFC (74.53%). Although the increase in water uptake is marginal, it shows that ionic nanoparticles help to increase the hydrophilicity of the dense layer. This is further confirmed by the water contact angle studies.

From the water contact angle analysis, it was observed that the water contact angle decreases from TFC to TFN-3. This shows that the hydrophilicity of the membranes increases due to the presence of ionic nanoparticles in the dense layer. The water contact of TFC is 42.8°, which reduces significantly to 29.6° in TFN-2. On further increasing the concentration of ionic nanoparticles in the dense layer, no significant reduction in water contact angle takes place as observed for TFN-3, which shows a water contact angle of 29.2°.

3.2.5 Surface roughness. The roughness of the surface of the membranes was determined by AFM analysis. From Fig. 7, it can be observed that the concentration of the nanoparticles increases with a concordant increase in the roughness parameters of the membrane. The roughness parameters taken into consideration were average roughness (R_a), root mean square roughness (R_q) and maximum peak to valley roughness (R_{max}) which are given in Table 3. The trend observed regarding the roughness of the membranes can be attributed to the hydrophilicity of the nanoparticles as it was proved from the higher hydrodynamic diameter from DLS analysis.[34] During the formation of the polyamide layer, it is believed that the nanoparticles dispersed in the organic solvent migrate towards the aqueous layer leading to the variation in the topography of the membrane surface.[45] The higher surface roughness of the membranes helps to improve the rejection capability of the membranes.

3.2.6 Zeta potential of the membranes:. The TFC membrane showed higher negative zeta potential values below pH 4 compared to the TFN-1 membrane (Fig. S9, ESI†). This

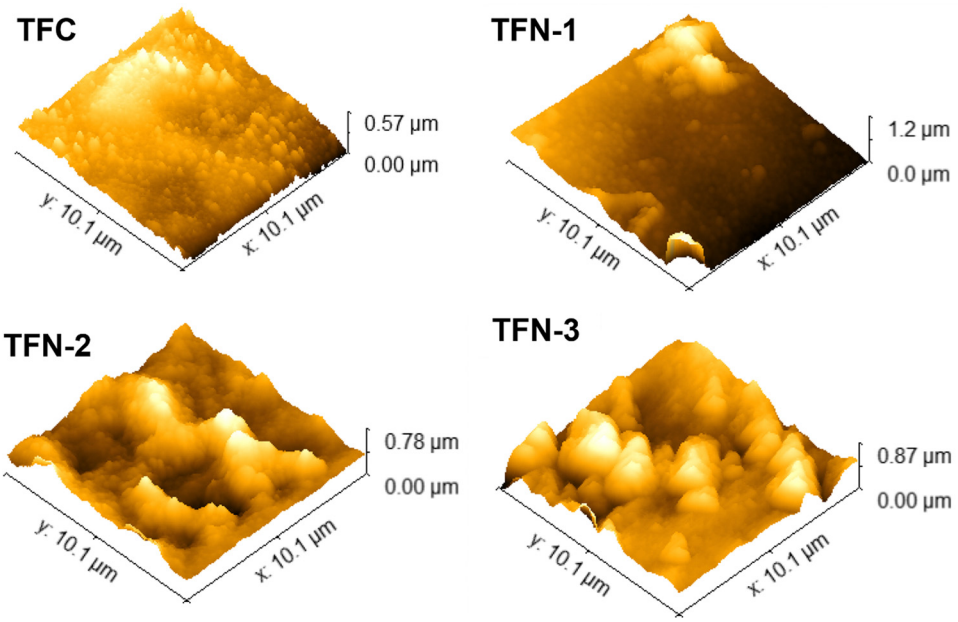

Fig. 7 AFM images displaying the surface roughness of the membranes.

could be attributed to the positive zeta potential exhibited by the poly(VBC-*co*-VI) nanoparticles. Hence, the better rejection property of the nanocomposite membranes towards the rejection of the anionic dyes could be ascribed to the electrostatic attraction between the dye molecules and the membranes. At pH 7 (the pH at which the dye rejection and salt rejection were carried out), the TFC membrane displayed a zeta potential of −47.09 mV, while the TFN-2 membrane displayed a zeta potential of −18.25 mV. The greater positive zeta potential of the TFN-2 membrane compared to the TFC helps in the repulsive interaction towards the Na^+ and Mg^{2+} ions.

3.2.7 Antifouling study. The antifouling study was conducted in terms of adsorption of a protein BSA of 0.8 mg mL^{-1} concentration. From Fig. S10 (ESI†), it can be observed that the addition of ionic nanoparticles in the PA layer increases the antifouling property appreciably in comparison to the neat TFC membrane. This is an interesting observation because the ionic nanoparticles possess a positive zeta potential of 23.8 mV, while the BSA protein has a negative zeta potential of around −30 mV at neutral pH.[46] This could be due to the formation of a hydration layer (as deduced from the EDS mapping of the nanoparticles as well as the OH peak in the FTIR spectrum) similar to that seen in zwitterionic nanoparticles which prevents the adsorption of the protein molecules on the membrane surface,[47] because the data obtained from the zeta potential of the membranes show the neat TFC membrane possessing a more negative zeta potential compared to TFN-2. The BSA adsorption on the neat TFC membrane was 150.82 μg cm^{-2}, while the adsorption of BSA on TFN-2 was reduced to 57.07 μg cm^{-2}. The adsorption of BSA on TFN-3 was nearly one-sixth of the BSA adsorption on TFC (23.54 μg cm^{-2}). This shows that the ionic nanoparticles possess a significant antifouling property.

4. Conclusions

Ionic poly(VBC-*co*-VI) nanoparticles were synthesized using the QPP method which proceeded *via* the free radical mechanism. The poly(VBC-*co*-VI) ionic nanoparticles were then incorporated into the PA layer of the TFC membranes *via* interfacial polymerization to give TFN membranes. The membranes showed appreciable rejection capability of the dyes RB5 (98%) and SY FCF (>95%) (100 ppm concentration) as well as salts NaCl (36%), $MgCl_2$ (>50%), Na_2SO_4 (85%) and $MgSO_4$ (85%) (1000 ppm concentration). An interesting observation was made concerning the membrane zeta potential and the antifouling study of the membrane, wherein the TFN-2 membrane having 0.05 wt% of the nanoparticles, showed a greater positive zeta potential compared to the neat TFC membrane. However, the TFN-2 membrane showed better antifouling property compared to the neat TFC membrane. This could be due to the formation of a hydration layer akin to zwitterionic nanoparticles which imparts their characteristic antifouling property. Hence, there is a need for more research into this class of nanoparticles and their potential applications in antifouling coating, drug delivery, chemical separation and other fields of research.

Data availability

The data supporting this article is available from the authors upon reasonable request.

Conflicts of interest

The authors declare that they have no known competing financial interests or personal relationships that could have appeared to influence the work reported in this paper.

Acknowledgements

AMI and NRM thank CRF NITK Surathkal, CAIF MAHE Manipal, MRC MNIT Jaipur and the Advanced Instrumentation Centre St. Aloysius (Deemed to be university), Mangalore for their support in the characterization of the nanoparticles and membranes. NRM thanks the DST, Government of India, for the INSPIRE Fellowship. AMI and NRM thank Dr Gurumurthy Hegde for his support in the analysis of the nanoparticles at Christ University, Bangalore.

References

1 R. Davarnejad, S. Afshar, M. Pirhadi and M. Mirhosseini, Mercury(II) adsorption process from an aqueous solution through activated carbon blended with fresh pistachio green shell powder, *Sci. Rep.*, 2025, 1–15.
2 B. Wang, P. Ma, M. Liu, R. Huang, Z. Qiu, L. Pan, J. Wang, Y. Liu and Q. Zhang, Enhancement of microalgae co-cultivation self-settling performance and water purification-capacity of microalgae biofilm, *Environ. Res.*, 2025, **265**, DOI: 10.1016/j.envres.2024.120342.
3 H. Peng, Y. Guo, G. Ma, X. Fan, K. Shu, Y. Li, J. Liao, N. Liu, F. Li and L. Ma, Hyperbranched phosphate functionalized covalent organic framework for high-performance recovery of ^{177}Lu from wastewater, *Sep. Purif. Technol.*, 2025, **361**, DOI: 10.1016/j.seppur.2024.131326.
4 S. Chen, S. Li, X. Yang, Y. Lu, L. Luo, J. Xu, K.-C. Ho and T. Luan, Application of algal-mycelial pellets in the treatment of the mariculture wastewater, *J. Environ. Sci.*, 2025, **154**, 128–137.
5 L. Yang, Z. Chen, Y. Tang and Q. Wen, Evaluation of magnetic ion-exchange resin for oxytetracycline removal in secondary effluent: behavior, mechanisms and theoretical calculation, *Sep. Purif. Technol.*, 2025, **361**, 131333.
6 P. Satishkumar, A. M. Isloor, L. N. Rao and R. Farnood, Fabrication of 2D Vanadium MXene Polyphenylsulfone Ultrafiltration Membrane for Enhancing the Water Flux and for Effective Separation of Humic Acid and Dyes from Wastewater, *ACS Omega*, 2024, **9**(24), DOI: 10.1021/acsomega.3c10078.
7 M. Kumar, A. M. Isloor, M. C. S. Nayak, S. R. Todeti, M. Padaki and A. F. Ismail, Hydrophilic polydopamine/polyvinylpyrrolidone blended polyphenylsulfone hollow

fiber membranes for the removal of arsenic-V from water, *J. Environ. Chem. Eng.*, 2023, **11**, 110358.
8 B. M. Ganesh, A. M. Isloor and A. F. Ismail, Enhanced hydrophilicity and salt rejection study of graphene oxide-polysulfone mixed matrix membrane, *DES*, 2013, **313**, 199–207.
9 S. Ibrahim, M. M. Ghaleni, A. M. Isloor, M. Bavarian and S. Nejati, Poly(Homopiperazine – Amide) Thin-Film Composite Membrane for Nano fi ltration of Heavy Metal Ions, *ACS Omega*, 2020, **5**(44), DOI: **10.1021/acsomega.0c04064**.
10 G. Ciardelli, L. Corsi and M. Marcucci, Membrane separation for wastewater reuse in the textile industry, *Resour., Conserv. Recycl.*, 2000, **31**, 189–197.
11 N. S. Naik, M. Padaki, A. M. Isloor, K. K. Nagaraja and K. A. Vishnumurthy, Poly(ionic liquid)-Based charge and size selective loose nanofiltration membrane for molecular separation, *Chem. Eng. J.*, 2021, **418**, 129372.
12 T. H. Kim, C. Park and S. Kim, Water recycling from desalination and purification process of reactive dye manufacturing industry by combined membrane filtration, *J. Cleaner Prod.*, 2005, **13**, 779–786.
13 H. Y. Lin and A. I. Schäfer, Adsorption of steroid hormone micropollutant by polyethersulfone ultrafiltration membranes with varying morphology, *Sep. Purif. Technol.*, 2025, **354**, DOI: **10.1016/j.seppur.2024.128733**.
14 G. P. S. Ibrahim, A. M. Isloor, Inamuddin, A. M. Asiri, A. F. Ismail, R. Kumar and M. I. Ahamed, Performance intensification of the polysulfone ultrafiltration membrane by blending with copolymer encompassing novel derivative of poly(styrene-*co*-maleic anhydride) for heavy metal removal from wastewater, *Chem. Eng. J.*, 2018, **353**, 425–435.
15 R. Kumar, A. M. Isloor, A. F. Ismail, S. A. Rashid and T. Matsuura, Polysulfone–Chitosan blend ultrafiltration membranes: preparation, characterization, permeation and antifouling properties, *RSC Adv.*, 2013, **3**, 7855–7861.
16 G. P. Syed Ibrahim, A. M. Isloor, A. F. Ismail and R. Farnood, One-step synthesis of zwitterionic graphene oxide nanohybrid: application to polysulfone tight ultrafiltration hollow fiber membrane, *Sci. Rep.*, 2020, **10**, DOI: **10.1038/s41598-020-63356-2**.
17 H. Yu, Y. Cao, G. Kang, J. Liu, M. Li and Q. Yuan, Enhancing antifouling property of polysulfone ultrafiltration membrane by grafting zwitterionic copolymer via UV-initiated polymerization, *J. Membr. Sci.*, 2009, **342**, 6–13.
18 G. P. Syed Ibrahim, A. M. Isloor, M. Bavarian and S. Nejati, Integration of Zwitterionic Polymer Nanoparticles in Interfacial Polymerization for Ion Separation, *ACS Appl. Polym. Mater.*, 2020, **2**, 1508–1517.
19 M. Kim, S.-J. Park and J.-H. Lee, Ultrahighly Li-selective nanofiltration membranes prepared via tailored interfacial polymerization, *J. Membr. Sci.*, 2024, **700**, 122728.
20 B. Khorshidi, T. Thundat, B. A. Fleck and M. Sadrzadeh, Thin film composite polyamide membranes: parametric study on the influence of synthesis conditions, *RSC Adv.*, 2015, **5**, 54985–54997.
21 N. Prabhakar, A. M. Isloor, R. Farnood and A. Fauzi Ismail, Fabrication and incorporation of MIL-53(Fe)-zwitterionic brushes into PVDF thin film composite membranes for enhancing heavy metal/dye rejection from aqueous body, *Sep. Purif. Technol.*, 2025, **358**, 1–16.
22 H. Mokarizadeh, S. Moayedfard, M. S. Maleh, S. I. G. P. Mohamed, S. Nejati and M. R. Esfahani, The role of support layer properties on the fabrication and performance of thin-film composite membranes: the significance of selective layer-support layer connectivity, *Sep. Purif. Technol.*, 2022, **278**, 119451.
23 J. Wang, Y. Huang, L. Xue, X. Gu, J. He, Y. Lu and C. Gao, Polyethylene based nanofiltration membranes with internally confined polyamide separating layers from cross substrate interface polymerization, *J. Membr. Sci.*, 2025, **717**, DOI: **10.1016/j.memsci.2024.123628**.
24 P. Li, Y. Zhou, C. Hai, Y. Tang, Y. Cheng, Y. Sun, S. Dong, L. Ma, X. He and Q. Xu, High-flux polyamide nanofiltration membranes tuning by polydopamine-modified boron nitride nanosheets: accelerating Mg^{2+}/Li^{+} separation, *Sep. Purif. Technol.*, 2025, **356**, 129917.
25 G. Feng, H. Zhang, J. Chen, Z. Fang and X. Hu, Modified graphene oxide (GO) embedded in nanofiltration membranes with high flux and anti-fouling for enhanced surface water purification, *J. Environ. Chem. Eng.*, 2025, **13**, 115172.
26 H. Zhang, Q. Liu, P. Zhou, H. Zhang, L. Xu, X. Sun and J. Xu, Co/SH-based MOFs incorporated nanofiltration membranes for efficient selenium uptake in water purification, *J. Hazard. Mater.*, 2025, **485**, DOI: **10.1016/j.jhazmat.2024.136836**.
27 L. Ba, C. Chen, R. Meng, Y. Chen, Y. Wu, Y. Liu, W. Huang, F. Yang, J. Cheng and X. Yi, A new method for the mitigation of piperazine transfer rate to prepared nanofiltration membranes by modified PVDF substrate through MOF-303@GO, *Sep. Purif. Technol.*, 2025, **361**, 131302.
28 H. Wen, Z. Liu, Z. Lu, Y. Yang and J. P. Chen, High-performance PEI-based nanofiltration membrane by MXene-regulated interfacial polymerization reaction: design, fabrication and testing, *J. Membr. Sci.*, 2025, **717**, 123568.
29 S. Dai, P. Wu, W.-S. Zou, W. Kong, X. Chen, J. Zhang, W. Li, X. Huang and Y. Wang, Biofouling/acid resistant nanofiltration membranes interfacially polymerized with nickel-doped carbon dots for highly efficient removal and real-time monitoring of chromate in wastewater, *J. Membr. Sci.*, 2025, **717**, 123581.
30 Y. Yan, J. Wang, W. Wang, C. Han, K. Huo, Q. Zhang and N. Wang, Efficient Li^{+}/Mg^{2+} separation nanofiltration membranes modified by amine-functionalized TiO_2 nanoparticles, *J. Environ. Chem. Eng.*, 2024, **12**, 113627.
31 G. Liu, Z. Pu, C. Matindi, Z. Cui, H. Wang, J. Yang and J. Li, Fabrication of charged and zwitterionic nanofiltration membranes and anti-adhesion analysis using quartz crystal microbalance with dissipation and atomic force microscopy, *J. Membr. Sci.*, 2025, **713**, 123292.
32 G. P. S. Ibrahim, A. M. Isloor, Inamuddin, A. M. Asiri and R. Farnood, Tuning the surface properties of Fe_3O_4 by zwitterionic sulfobetaine: application to antifouling and

dye removal membrane, *Int. J. Environ. Sci. Technol.*, 2020, **17**, 4047–4060.

33 X. Mao, N. Xu, X. Shi, H. Wen and C. Liu, Integration of charge repulsion and size exclusion effects into the skin layer matrix for enhanced Mg^{2+}/Li^{+} nanofiltration separation, *J. Membr. Sci.*, 2025, **713**, 123315.

34 S. I. Gnani Peer Mohamed, A. M. Isloor and R. Farnood, Catalyst- and Stabilizer-Free 7Rational Synthesis of Ionic Polymer Nanoparticles in One Step for Oil/Water Separation Membranes, *ACS Appl. Mater. Interfaces*, 2022, **14**, 45800–45809.

35 K. N. Mahadevaprasad, K. N. Santhosh, K. A. Kumar and S. K. Nataraj, Mn-aminoclay induced biopolymer interfacial TFC membrane for emerging pollutants separation and effective heavy metal sequestration, *Chem. Eng. J.*, 2025, **504**, DOI: **10.1016/j.cej.2024.158717**.

36 L. Zhang, Y. Tang, X. Sun, G. Xia and X. Zhou, Capsaicin mimic-based antifouling and antibacterial polyester nanofiltration membranes with tunable crosslinked structures, *J. Environ. Chem. Eng.*, 2024, **12**, 113774.

37 L. Dong, H. Li and L. Cheng, Single Walled Carbon Nanotube/Carboxymethyl Cellulose – Based Polyester Composite Nanofiltration Membrane for Enhanced Water Purification, *Water, Air, Soil Pollut.*, 2024, **235**, 1–14.

38 Y. Zhang, X. Tian, J. Han, X. Zhang, Y. Gao and G. Naren, Synthesis of Cu-doped Ni-B amorphous alloy catalyst and its catalytic performance for BH – 4 oxidation, *Arabian J. Chem.*, 2025, **18**, 106059.

39 M. Thommes, K. Kaneko, A. V. Neimark, J. P. Olivier, F. Rodriguez-Reinoso, J. Rouquerol and K. S. W. Sing, Physisorption of gases, with special reference to the evaluation of surface area and pore size distribution (IUPAC Technical Report), *Pure Appl. Chem.*, 2015, **87**, 1051–1069.

40 C. Zhan and S. C. Jana, Solid state polymer ionogel electrolyte for use in Li-ion batteries, *SPE Polym.*, 2020, 55–65.

41 A. El Hoshoudy, Synthesis and Characterization of Polyacrylamide Crosslinked Copolymer for Synthesis and Characterization of Polyacrylamide Crosslinked Copolymer for Enhanced Oil Recovery and Rock Wettability Alteration, *Int. J. Oil, Gas Coal Eng.*, 2015, **3**(4), DOI: **10.11648/j.ogce.20150304.11**.

42 P. Hu, H. Song, Z. Xu, S. Zhao, X. Zhang, B. Yuan and Q. J. Niu, Ultra-permeable thin-film nanocomposite membrane with an asymmetric structure harvested by a heterogeneous interlayer for brackish water desalination, *Desalination*, 2024, **586**, DOI: **10.1016/j.desal.2024.117896**.

43 I. Shefer, O. Peer-Haim and R. Epsztein, Limited ion-ion selectivity of salt-rejecting membranes due to enthalpy-entropy compensation, *Desalination*, 2022, **541**, 116041.

44 S. M. Bannon, E. Kutner, B. Garretson and G. M. Geise, Understanding the influence of sodium chloride concentration on ion diffusion in charged polymers, *J. Membr. Sci.*, 2024, **712**, 123197.

45 P. Qu, H. Tang, Y. Gao, L. P. Zhang and S. Wang, Polyethersulfone composite membrane blended With cellulose fibrils, *BioResources*, 2010, **5**, 2323–2336.

46 M. Férová, P. Rusnok and R. Marsalek, Mathematical Methods in the Calculation of the Zeta Potential of BSA, *J. Solution Chem.*, 2018, **47**, DOI: **10.1007/s10953-018-0830-0**.

47 D. Sun, P. Li, X. Li and X. Wang, Protein-resistant surface based on zwitterion-functionalized nanoparticles for marine antifouling applications, *New J. Chem.*, 2020, **44**, 2059–2069.

